Check for updates

ADVANCED FUNCTIONAL MATERIALS
www.afm-journal.de

Mechanochemically Activatable Liquid Metal Powders for Sustainable, Reconfigurable, and Versatile Electronics

Osman Gul, Junseong Ahn, Hye Jin Kim, Xinge Yu,* and Inkyu Park**

While liquid metals possess exceptional electrical conductivity, their integration into stretchable and recyclable electronics remains constrained. High surface tension causes poor adhesion and uncontrolled spreading, and current processing methods often lack scalability or recyclability, limiting broader adoption in soft robotics, wearable healthcare, and sustainable systems. Here, a class of mechanochemically activatable liquid metal powders (MALMPs) is introduced that decouple conductivity from fluidity, enabling ambient stable, recyclable, and user-defined soft circuits. Sonication dispersion of eutectic gallium–indium in carbonyl-rich solvents yields core–shell particles with oxide-stabilized surfaces. These powders remain electrically inert under ambient conditions but can be locally activated by mechanical pressure, which ruptures the shell to restore conductivity. This mechanism allows dry-state patterning on a wide range of substrates, including flexible, stretchable, and biological surfaces, followed by localized fluidization upon mechanical activation to induce conductivity. MALMPs maintain stable conductivity under >10 000 stretching cycles and 700% strain and can be fully recycled via mild sodium hydroxide (NaOH) treatment. Demonstrations across transient and reconfigurable circuits, human–machine interfaces, and skin-conformal systems highlight the versatility and scalability of the platform for next-generation electronics.

1. Introduction

Stretchable[1–3] reconfigurable,[4–6] and recyclable[7–10] electronics are increasingly important for advancing wearable devices,[11–14] soft robotics,[15–17] and sustainable device technologies.[18–20] Among the candidate materials for such systems, eutectic gallium–indium (EGaIn) liquid metal alloys have attracted substantial attention due to their high conductivity, intrinsic deformability, and biocompatibility.[21–31] However, the practical deployment of liquid metals (LMs) remains hindered by their high surface tension, which prevents effective wetting on most surfaces, leading to poor adhesion and unstable patterning (Movie S1, Supporting Information).[32–36]

In recent years, LM-based inks have emerged as promising candidates for patterning on various substrates.[37–40] Veerapandian et al. introduced intrinsically conductive hydrogen-doped LM microparticles that exhibit stable and reliable electrical conductivity.[41] However, the ink formulation is based on organic solvents and requires post-deposition thermal annealing at 120 °C for 3 h to remove residual solvents and induce surface passivation. These processing conditions limit compatibility with diverse substrates and constrain practical deployment in rapid or low-temperature fabrication environments. Other strategies focus on integrating LM particles directly into the substrate to enable embedded circuit architecture. For instance, Seo et al. developed a ligand-assisted LM particle system that facilitates one-step fabrication of self-packaged, stretchable multilayer circuits via in situ sintering and vertical phase separation.[2] Additionally, Ho et al. demonstrated a scalable approach for 3D assembly of electrical interconnects by leveraging gravity-driven stratification of LM microdroplets in a photocurable resin, enabling multilayer interconnects without through-hole drilling.[42] However, these techniques result in circuits that become permanently encapsulated upon curing and activation, precluding post-fabrication repair or reconfiguration. This irreversible architecture limits their applicability in adaptive or recyclable electronic systems that demand circuit-level modularity. A recent study introduces a LMs–vitrimer conductive composite that utilizes dynamic covalent bonding to achieve recyclability, self-healing, and reconfigurable electrical functionality within a rigid, plastic-like matrix.[43] However, the composite is fundamentally limited to vitrimer-based substrates, as its

O. Gul, I. Park
Department of Mechanical Engineering
Korea Advanced Institute of Science and Technology (KAIST)
291 Daehak-ro, Yuseong-gu, Daejeon 34141, Republic of Korea
E-mail: inkyu@kaist.ac.kr
J. Ahn
Department of Control and Instrumentation Engineering
Korea University
Sejong 30019, Republic of Korea
H. J. Kim
Intelligent Components and Sensors Research Section
Electronics and Telecommunication Research Institute (ETRI) 218 Gajeong-ro
Yuseong-gu, Daejeon 34129, Republic of Korea
E-mail: nolawara@etri.re.kr
H. J. Kim
Department of Advanced Device Technology
University of Science and Technology
Daejeon 34113, Republic of Korea
X. Yu
Department of Biomedical Engineering
City University of Hong Kong
Hong Kong, SAR 999077, China
E-mail: xingeyu@cityu.edu.hk

The ORCID identification number(s) for the author(s) of this article can be found under https://doi.org/10.1002/adfm.202527396

DOI: 10.1002/adfm.202527396

 © 2025 Wiley-VCH GmbH

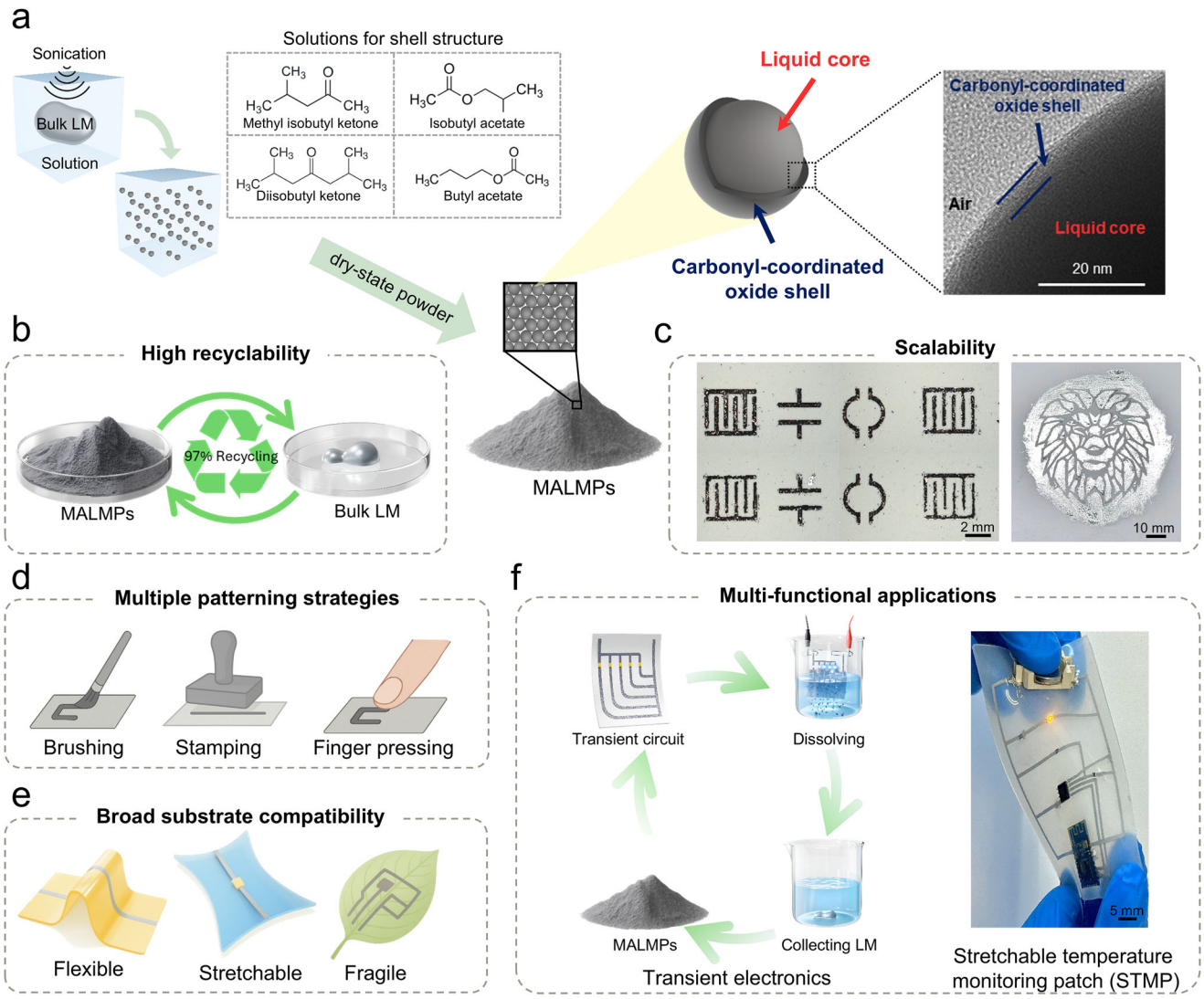


Figure 1. Overview of mechanochemically activatable liquid metal powders (MALMPs) and their applications: a) Schematic illustration of the fabrication and of MALMPs via solvent-mediated sonication, yielding dry, core–shell structured particles and TEM image of MALMPs. b) Schematic illustration of the MALMPs recycling process, demonstrating a 97% material recovery rate. c) High-resolution patterning of MALMPs on both micro- and large-area scales. d) Multiple patterning strategies can be applied to MALMPs, including brushing, stamping, and finger pressing. e) Universal substrate compatibility demonstrated across diverse materials, including flexible, stretchable, and fragile substrates. f) Demonstrations of MALMPs-enabled multifunctional electronics: from transient electronics to stretchable wireless temperature monitoring patch.

recyclability and interfacial integrity rely on transesterification reactions that are not compatible with conventional thermosets, thermoplastics, or elastomeric materials, thereby restricting its integration with a broader range of device platforms. Despite the many efforts so far, LMs-based solutions that enable patterning on diverse substrates while being recyclable and reconfigurable still need notable progress (Table S1, Supporting Information).

Here, we report a new class of Mechanochemically Activatable Liquid Metal Powders (MALMPs) that offers reconfigurable conductivity, ambient stability, compatibility with diverse substrate patterning, and complete material recyclability, overcoming the major limitations of LM-based conductive materials. These MALMPs are synthesized via solvent-assisted sonication of EGaIn in selected carbonyl-rich organic solvents such as methyl isobutyl ketone (MIBK), diisobutyl ketone (DIBK), and isobutyl acetate (**Figure 1a**). This process generates core–shell micro- and nanoparticles, where the metallic core is stabilized by a passivating oxide shell coordinated with solvent-derived carbonyl ligands. The synthesized powders exhibit a dry and electrically insulating nature, maintaining stability under ambient conditions. Notably, they can be repeatedly reprocessed through shell dissolution followed by particle regeneration via sonication. The MALMPs can be easily recycled, achieving a 97% recycling rate (Figure 1b).

Upon mechanical activation, the oxide shell locally ruptures to allow direct metal–metal contact and instantaneous restoration of high conductivity (Movies S2 and S3, Supporting Information). This mechanochemical switching provides direct user-defined control of circuit formation without requiring heat, current, or

© 2025 Wiley-VCH GmbH

16163028, 2026, 22, Downloaded from https://advanced.onlinelibrary.wiley.com/doi/10.1002/adfm.202527396 by Korea University Library, Wiley Online Library on [29/03/2026]. See the Terms and Conditions (https://onlinelibrary.wiley.com/terms-and-conditions) on Wiley Online Library for rules of use; OA articles are governed by the applicable Creative Commons License

16163028, 2026, 22, Downloaded from https://advanced.onlinelibrary.wiley.com/doi/10.1002/adfm.202527396 by Korea University Library, Wiley Online Library on [29/03/2026]. See the Terms and Conditions (https://onlinelibrary.wiley.com/terms-and-conditions) on Wiley Online Library for rules of use; OA articles are governed by the applicable Creative Commons License

additional chemicals, facilitating patterned circuit design on demand. The MALMPs support high-fidelity patterning across both micro- and macroscale geometries (Figure 1c). The MALMPs can be activated through stamping, finger pressing, or brushing, offering the advantage of multiple patterning strategies (Figure 1d). The MALMPs demonstrate universal substrate compatibility, adhering conformally to soft, rigid, stretchable, fragile, biodegradable, and even 3D curved surfaces (Figure 1e). The MALMPs exhibit robust environmental and mechanical durability, retaining performance under repeated deformation, heating, and long-term storage (up to a year). To demonstrate the functional breadth of the platform, we integrated MALMPs into a range of proof-of-concept devices, including a transient LED array, a human–machine interface, a pressure-responsive logic circuit, and a stretchable temperature monitoring patch (STMP), each showcasing the system's programmability, reusability, and on-demand activation capabilities (Figure 1f). Together, these examples highlight a materials strategy that enables scalable, recyclable, and mechanically reconfigurable electronics. By uniting dry-state processability, pressure-triggered conductivity, and closed-loop material recyclability, the MALMPs platform establishes a versatile foundation for next-generation soft, sustainable, and adaptive electronic systems.

2. Results and Discussion

2.1. Structural and Chemical Characterization of MALMPs

The synthesized MALMPs exhibit a characteristic core–shell morphology, originating from the spontaneous oxidation of bulk EGaIn during sonication in oxygen-rich organic solvents (**Figure 2a**). Elemental mapping via energy-dispersive X-ray spectroscopy (EDS) confirms that gallium and indium are concentrated within the metallic core, while oxygen is enriched at the outer shell, consistent with the formation of a passivating gallium-based oxide layer (Figure 2b). The oxide layer thickness on the MALMPs surface increases by ≈55.6% compared to that of LM particles sonicated in IPA, as shown in Figure 2c. High-resolution X-ray photoelectron spectroscopy (XPS) reveals significant surface chemical evolution following sonication (Figure 2d,e; Figure S1, Supporting Information). The O 1s spectra of MALMPs exhibit enhanced non-lattice oxygen components, indicative of surface hydroxylation and complex coordination environments. In the C 1s region, intensified signals corresponding to C—O and C═O species are observed, suggesting that residual carbonyl-containing solvents, specifically MIBK, DIBK, isobutyl acetate, and butyl acetate, remain partially coordinated at the particle surface. Carbonyl groups (as soft Lewis bases) interact with Lewis acidic Ga^{3+} sites, forming ligand-like surface complexes that stabilize the oxide shell and modulate interfacial energy.[41,44–48] This interpretation is corroborated by the Ga 3d and In 3d spectra, which show increased Ga^{3+} and In^{3+} signals in the MALMPs compared to pristine EGaIn.

Fourier-transform infrared (FTIR) spectroscopy supports this coordination mechanism. The selected solvents exhibit strong C═O stretching bands near 1725 cm^{-1} and C—H stretches ≈2900 cm^{-1} (Figure 2f; Figure S2, Supporting Information), which are retained and amplified in the FTIR spectrum of MALMPs (Figure 2g). The persistence and enhancement of these carbonyl signals, absent in bulk EGaIn, suggest stable coordination at the Ga-oxide interface. Together with XPS findings, these results support a model in which surface Ga^{3+} centers coordinate with solvent-derived carbonyl ligands to form a chemically hybridized passivation layer.

During sonication, partial oxidation of Ga generates Ga^{3+} species at the droplet surface, which then interact with electron-rich carbonyl oxygen atoms to form $[Ga–O═C—R]^{n+}$ complexes. These interactions stabilize the shell, prevent coalescence, and promote colloidal stability. To rationalize the solvent-dependent success in powder formation, we analyzed the physicochemical properties of the four most effective solvents used in MALMP synthesis (Table S2, Supporting Information). All selected solvents possess moderate polarity (3.3–3.9), carbonyl-based coordination sites (ketone or ester groups), and low-to-medium volatility. Importantly, solvents with bulky or long hydrophobic tails (e.g., DIBK, isobutyl acetate) consistently produced light particle dispersions with stable heavy slurry phases during sonication, and ultimately yielded dry, flowable powders upon solvent evaporation. These observations suggest that both molecular coordination via the carbonyl group and physical properties, such as reduced volatility and steric hindrance, play essential roles in stabilizing the oxide shell and preventing particle agglomeration. The incorporation of bulky or linear long-chain alkyl tails likely mitigates surface energy mismatch between the particles and surrounding interfaces, thereby facilitating efficient dry powder recovery without aggregation or adhesion. These findings establish a rational framework for the mechanochemical synthesis of MALMPs: solvent selection governs not only the formation of the oxide shell via Ga^{3+}, ligand complexation, but also determines the final material phase, stability, and processability of the powders.

2.2. Processing and Recyclability

To enable scalable and environmentally sustainable use of MALMPs, we developed a simple and reversible fabrication strategy based on solvent-assisted sonication followed by solvent evaporation (**Figure 3a**). To systematically identify effective solvents for MALMPs synthesis, we screened 13 different candidates, including alcohols, ketones, and esters (Table S1, Supporting Information). The fabrication outcomes associated with each solvent are summarized in Figure S3, Supporting Information. Notably, sonication of EGaIn in NaOH solution, deionized water, or nonpolar solvents such as toluene did not produce any powder; the metal remained in its bulk liquid form. Similarly, polar protic solvents such as isopropanol, ethanol, and methanol, along with solvents like chloroform, acetone, and ethyl acetate, generated unstable LM slurries but failed to yield dry powders. In contrast, four solvents, MIBK, DIBK, isobutyl acetate, and butyl acetate, consistently produced dry, free-flowing, and stable MALMPs upon solvent evaporation. These effective solvents share key physicochemical characteristics, including moderate polarity, carbonyl-based coordination sites, and relatively low volatility, which appear critical for oxide shell stabilization and particle separation during sonication. The results corroborate the surface chemistry insights shown in Figure 2, highlighting that efficient powder formation arises from a synergistic interplay between mechanical fragmentation and solvent-mediated chemical

 © 2025 Wiley-VCH GmbH

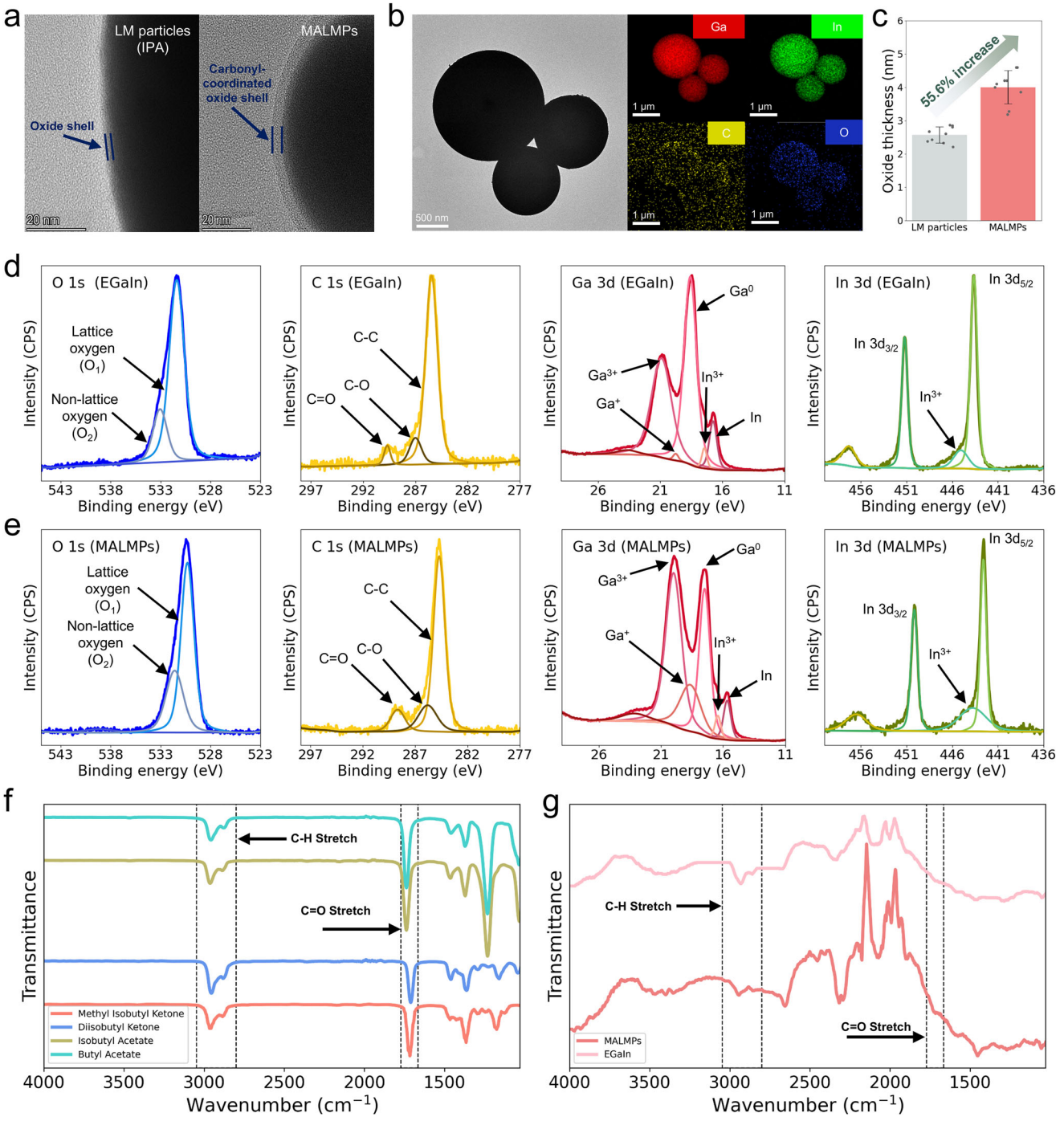


Figure 2. Core–shell structure and surface chemistry of MALMPs. a) TEM images showing LM particles (sonicated in IPA) and MALMPs with a core–shell structure. b) EDS analyses showing Ga, In, C, and O compositions of the MALMPs. c) Oxide layer thickness of LM particles and MALMPs. Data are presented as mean values ± SD, where $n = 9$, 3 technical replicates. Values are presented as means ± SD. Overall, MALMPs exhibited a 55.6% increase in thickness, attributed to the presence of a carbonyl-coordinated oxide shell, compared to unmodified LM particles. d) XPS spectra of O 1s, C 1s, Ga 3d, In 3d of EGaIn. e) XPS spectra of O 1s, C 1s, Ga 3d, In 3d of MALMPs surfaces. Compared to pristine EGaIn, MALMPs exhibited increased carbonyl (C═O) and non-lattice oxygen (O_2) signals along with a higher ratio of oxidized gallium (Ga^{3+}) and indium (In^{3+}), indicating enhanced surface oxidation and carbonyl coordination on the oxide shell. f) FTIR spectra of the solvents (MIBK, DIBK, isobutyl acetate, and butyl acetate). g) FTIR spectra of the EGaIn and MALMPs. The FTIR spectra reveal that MALMPs exhibit distinct C═O and C—H stretching bands, indicating successful incorporation of solvent-derived carbonyl functionalities on the oxide surface, unlike pristine EGaIn.

© 2025 Wiley-VCH GmbH

16163028, 2026, 22, Downloaded from https://advanced.onlinelibrary.wiley.com/doi/10.1002/adfm.202527396 by Korea University Library, Wiley Online Library on [29/03/2026]. See the Terms and Conditions (https://onlinelibrary.wiley.com/terms-and-conditions) on Wiley Online Library for rules of use; OA articles are governed by the applicable Creative Commons License

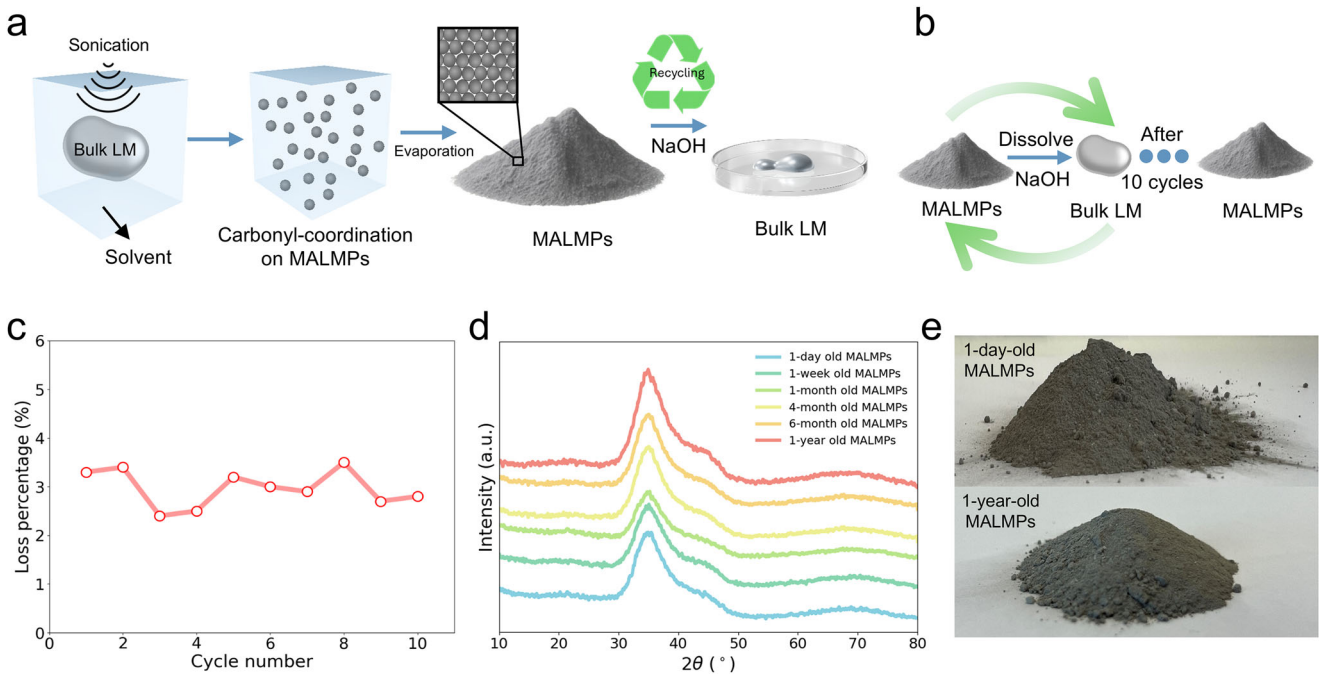


Figure 3. Fabrication, recyclability, and long-term stability of MALMPs. a) Schematic illustration of the solvent-assisted fabrication of MALMPs via sonication and solvent evaporation. NaOH-based chemical recycling process that enables recovery of the pristine EGaIn from the MALMPs, demonstrating recyclability. b) Schematic illustration of the MALPMs recycling process repeated over ten cycles. c) Mass loss percentage of MALMPs over ten recycling cycles. d) X-ray diffraction (XRD) patterns of MALMPs aged for different durations (1 day to 1 year), showing consistent phase characteristics and structural preservation. e) Photographs comparing the macroscopic appearance of 1-day-old and 1-year-old MALMPs, demonstrating excellent shelf-life and powder stability.

coordination at the metal interface. Specifically, FTIR and XPS results (Figure 2e,f) show that carbonyl-containing solvents such as MIBK, DIBK, and isobutyl/butyl acetate contain electron-rich ligands capable of coordinating with Ga^{3+} sites formed during sonication. The resulting $[Ga–O{=}C{-}R]^{n+}$ surface complexes stabilize the oxide shell and reduce interfacial energy, effectively suppressing coalescence and promoting colloidal stability. In contrast, solvents lacking strong donor groups (e.g., toluene) or those that are excessively volatile or polar (e.g., methanol, acetone) do not support sufficient coordination or shell formation, resulting in unstable dispersions. Furthermore, the presence of branched or linear alkyl chains in effective solvents such as DIBK and isobutyl acetate likely contributes to reduced surface energy and steric stabilization, aiding in dry powder recovery. Importantly, the entire fabrication process is recyclable through a mild NaOH-based chemical treatment that selectively dissolves the oxide shell, enabling the recovery of pristine EGaIn without altering its core properties (Movie S4, Supporting Information). Figure S4 (Supporting Information) captures the intermediate state immediately after sonication, showing distinct phase separation between light, dispersed particles, and a heavier slurry prior to solvent evaporation. After evaporation, the MALMPs formed dry-state powder particles. Their particle size distribution was characterized using scanning electron microscopy (SEM), with a representative image presented in Figure S5a, Supporting Information. The distribution (Figure S5b, Supporting Information) exhibits a mean diameter of 17.67 µm with a standard deviation of 11.28 µm, indicating a moderately broad size variation. To quantitatively evaluate long-term recyclability, a ten-cycle recycling experiment was performed. A schematic illustration of the process is presented in Figure 3b, and a detailed photographic sequence of all ten fabrication–recycling steps is shown in Figure S6, Supporting Information. The mass loss over the ten complete recycling cycles remained below 3%, confirming high material retention and excellent recyclability (Figure 3c). A step-by-step photographic sequence illustrates the full fabrication–dissolution–recovery loop, including sonication, solvent evaporation, NaOH treatment, and powder regeneration. Notably, even after ten full cycles and one year of ambient storage, the regenerated MALMPs remained physically intact and functionally reprocessable (Movie S5, Supporting Information). Further XPS analysis of the recycled MALMPs showed no detectable Na 1s signal, and the spectra closely matched those of pristine MALMPs, confirming that the NaOH treatment does not introduce residual sodium or other impurities during recycling, as shown in Figure S7, Supporting Information. Consistent with these findings, electrical measurements demonstrated that the post-activation conductivity of MALMPs remained stable over ten recycling cycles, maintaining a value of approximately $\approx 8.5 \times 10^5$ S m^{-1}, indicating that repeated recycling does not degrade their intrinsic electrical performance (Figure S8, Supporting Information). To assess structural integrity over time, X-ray diffraction (XRD) was performed on MALMPs stored for 1 day to 1 year (Figure 3d). All samples exhibited consistent diffraction profiles, with no emergence of crystalline oxide peaks or secondary phases, indicating the long-term stability of the amorphous oxide shell. Photographs comparing the macroscopic appearance of 1-day-old and 1-year-old powders (Figure 3e) revealed no significant changes in color,

© 2025 Wiley-VCH GmbH

16163028, 2026, 22, Downloaded from https://advanced.onlinelibrary.wiley.com/doi/10.1002/adfm.202527396 by Korea University Library, Wiley Online Library on [29/03/2026]. See the Terms and Conditions (https://onlinelibrary.wiley.com/terms-and-conditions) on Wiley Online Library for rules of use; OA articles are governed by the applicable Creative Commons License

texture, or powder flowability, further validating the excellent shelf-life and stability of the MALMPs. Movie S6 (Supporting Information) shows that the MALMPs retain full functionality even after one year of storage, exhibiting no signs of degradation. The long-term electrical reliability of MALMPs was further examined by comparing their activation and post-activation conductivity after extended ambient storage. As shown in Figure S9 (Supporting Information), the activation pressure–conductivity profiles of freshly prepared (1-day-old) and 1-year-old MALMPs exhibit similar mechanochemical switching behavior, with a sharp conductivity rise occurring between 200 and 300 kPa. Although the 1-year-old sample shows a modestly delayed activation onset, both samples converge to comparable saturation conductivities of $\approx 3.4 \times 10^5$ and $\approx 3.1 \times 10^5$ S m^{-1}, respectively, demonstrating that the pressure-triggered activation mechanism remains fully preserved after long-term storage. During the activation-pressure experiments, the MALMPs were compressed with a tip, producing a nonuniform layer that resulted in lower conductivity than the more uniform brush-patterned traces. Complementary measurements in Figure S10 (Supporting Information) further confirm that the post-activation conductivity of MALMP electrodes remains nearly unchanged ($\approx 8.5 \times 10^5$ S m^{-1}) for samples stored for 1 day, 6 months, and 1 year, indicating excellent long-term electrical stability. This stable conductivity, combined with the unchanged phase characteristics and surface chemistry validated by XRD and XPS (Figure 3d; Figures S1 and S7, Supporting Information), confirms that neither prolonged storage nor the recycling process introduces impurities or structural degradation. These results demonstrate that the solvent-assisted MALMPs fabrication method is not only scalable and recyclable but also provides long-term material stability and repeatable recovery, key features for practical use in transient, recyclable, and sustainable electronics.

2.3. Substrate Adaptability and Scalable Patterning

To demonstrate the practical versatility of MALMPs, we investigated their patternability and electrical performance across a wide range of substrates (**Figure 4**). Using a simple stamp-transfer method, MALMPs were conformally activated and patterned onto nonplanar or deformable substrates such as natural leaves, PMMA, woven fabrics, stainless steel, PET, and paper (Figure 4a; Figure S11, Supporting Information). In parallel, brush-based patterning enabled rapid circuit formation on rigid and curved substrates, including glass, poly(vinyl chloride) (PVC), silicon wafers, water-soluble paper, nitrile gloves, and copper foil (Figure 4b; Figure S12, Supporting Information). In all cases, the MALMPs exhibited strong substrate adhesion and high pattern fidelity without requiring surface pretreatment. The strong adhesion of MALMPs arises from the carbonyl-rich oxide shell and mechanically assisted wetting. Carbonyl ligands coordinate with Ga^{3+} to form a hybrid shell enriched in C═O and O– species, which interact strongly with hydroxylated or polar substrates through hydrogen bonding and dipole–dipole interactions.[49] Upon mechanical activation, rupture of the shell exposes low-surface-tension EGaIn, enabling transient wetting and mechanical interlocking with the microscale surface roughness features on the substrate.

We further assessed the mechanical integrity and uniformity of activated MALMPs traces on flexible PET films (Figure 4c). The optical microscope image confirms smooth edge profiles and a uniform electrode width of ≈80 μm. Cross-sectional analysis revealed a pattern thickness of ≈5 μm (Figure S13, Supporting Information), indicating compact, low-profile conduction paths suitable for thin, flexible electronics. This conformal behavior extended to complex biological surfaces, as demonstrated by an MALMP circuit printed directly onto a lemon, which successfully powered LEDs, highlighting 3D surface adaptability (Figure 4d). Stamping enables rapid deposition but yields broader features (≈500 μm), making it suitable for large-area patterning. In contrast, brush-based patterning achieves much finer geometries (≈80 μm) with high uniformity, providing the resolution needed for dense and precise interconnects. To evaluate mechanical activation thresholds, we measured the pressure required to transition MALMPs from non-conductive to conductive states. The activation pressure ranged from 215 to 335 kPa, well within the range of moderate finger pressing, indicating suitability for user-interactive and wearable applications (Figure S14, Supporting Information). The electrical performance of LMP traces was further validated across ten representative substrates, including paper, PMMA, wood, fabric, polyimide, silicon wafer, glass, PET, polypropylene (PP), and polyethylene (PE) (Figure 4e). All substrates supported stable conductivity on the order of 10^5 S/m, with minor variations attributed to differences in surface roughness and porosity. Finally, we demonstrated a fully functional LED array printed on paper using MALMPs-based interconnects, showcasing practical integration and real-world applicability (Figure 4f). These results underscore the broad material compatibility, mechanical adaptability, and electrical robustness of MALMPs, positioning them as promising candidates for printable and flexible electronic systems.

2.4. Robust Circuit Material Based on MALMPs

To evaluate the mechanical, electrical, and environmental reliability of MALMPs-based conductive electrodes, we conducted systematic testing under various deformation and ambient conditions (**Figure 5**). MALMPs printed on a fabric substrate retained line uniformity and electrical continuity (Figure 5a). Bending tests showed negligible change in relative resistance ($\Delta R/R_0$) down to a bending radius of 2.5 mm (Figure 5b), while cyclic bending over 10 000 repetitions confirmed stable electrical performance and minimal mechanical fatigue (Figure 5c). Similarly, twisting the MALMPs electrodes through 360° resulted in no significant resistance drift, indicating high torsional robustness (Figure 5d). The MALMPs circuits also demonstrated strong thermal stability, exhibiting only a 7% relative resistance increase from 20 to 100 °C. This minimal thermal sensitivity highlights their reliability for temperature-varying environments (Figure 5e). Ambient aging studies over 30 days under uncontrolled laboratory humidity showed no measurable degradation in electrical performance, supporting long-term environmental durability (Figure 5f). We further tested the stretchability of activated MALMPs on elastomeric substrates (Ecoflex), where the traces exhibited stable conduction up to 700% uniaxial strain, with the normalized resistance (R/R_0) increasing moderately to

© 2025 Wiley-VCH GmbH

16163028, 2026, 22, Downloaded from https://advanced.onlinelibrary.wiley.com/doi/10.1002/adfm.202527396 by Korea University Library, Wiley Online Library on [29/03/2026]. See the Terms and Conditions (https://onlinelibrary.wiley.com/terms-and-conditions) on Wiley Online Library for rules of use; OA articles are governed by the applicable Creative Commons License

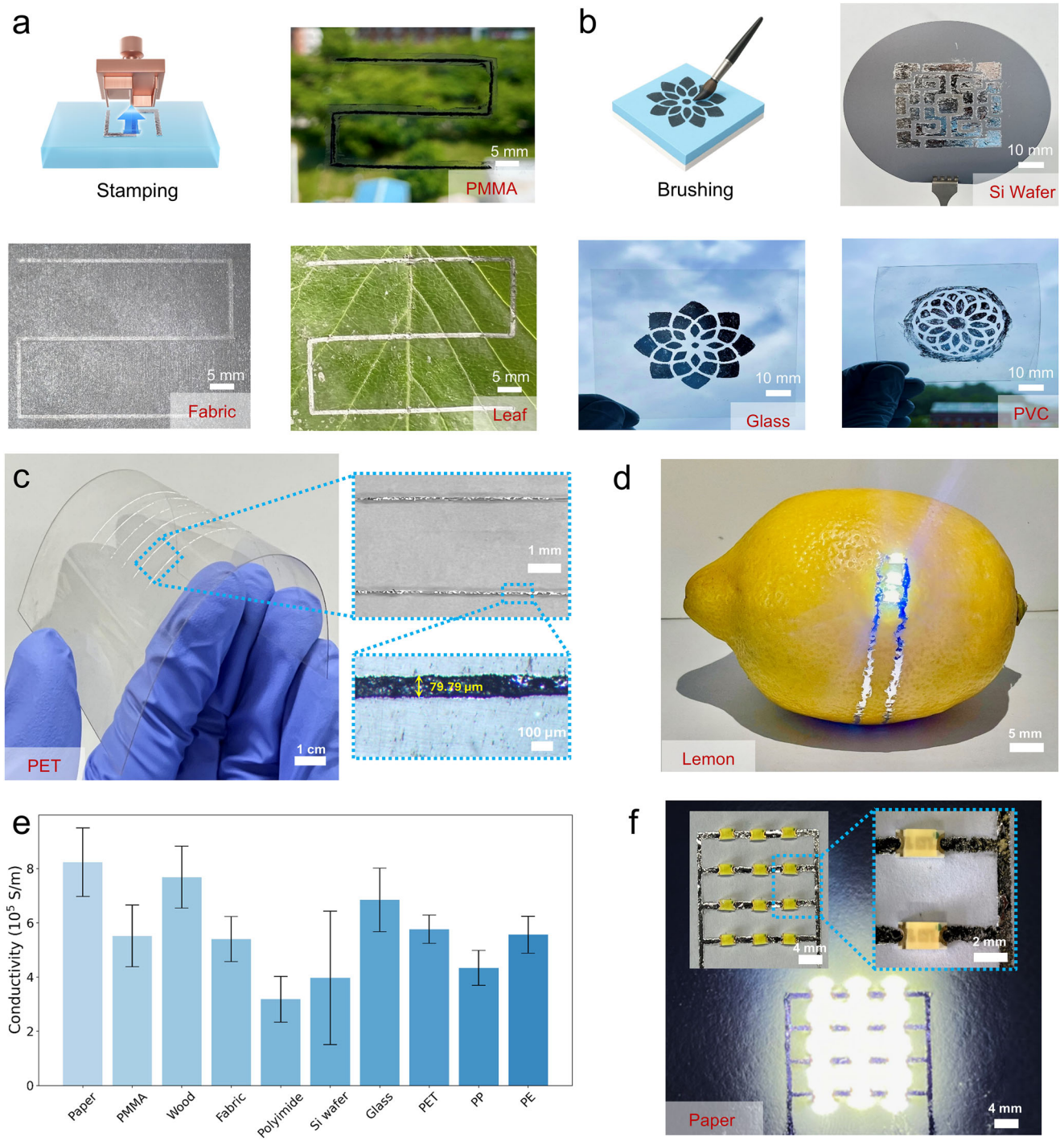


Figure 4. Substrate adaptability and patterning of MALMPs-based conductive electrodes. a) Demonstration of stamp-based patterning of MALMPs on nonplanar and soft substrates such as plant leaf, PMMA, and fabric. b) Brush-based circuit patterning on rigid and curved substrates such as glass, PVC, and a silicon wafer. c) Optical images of MALMP patterns on a flexible PET film, showing stretchable and foldable conformance along with top-view magnified images of line geometry and uniform trace width (≈80 µm). d) Functional circuit printed on a lemon, lighting up blue LEDs to demonstrate 3D conformal adhesion. e) Electrical conductivity of MALMP electrodes measured on various substrates, showing stable performance across paper, PMMA, wood, fabric, polyimide, silicon wafer, glass, PET, PP, and PE. Data are presented as mean values ± SD, where $n = 3$ technical replicates. f) Integrated LED array on a paper substrate using MALMP interconnects, demonstrating practical implementation.

© 2025 Wiley-VCH GmbH

16163028, 2026, 22, Downloaded from https://advanced.onlinelibrary.wiley.com/doi/10.1002/adfm.202527396 by Korea University Library, Wiley Online Library on [29/03/2026]. See the Terms and Conditions (https://onlinelibrary.wiley.com/terms-and-conditions) on Wiley Online Library for rules of use; OA articles are governed by the applicable Creative Commons License

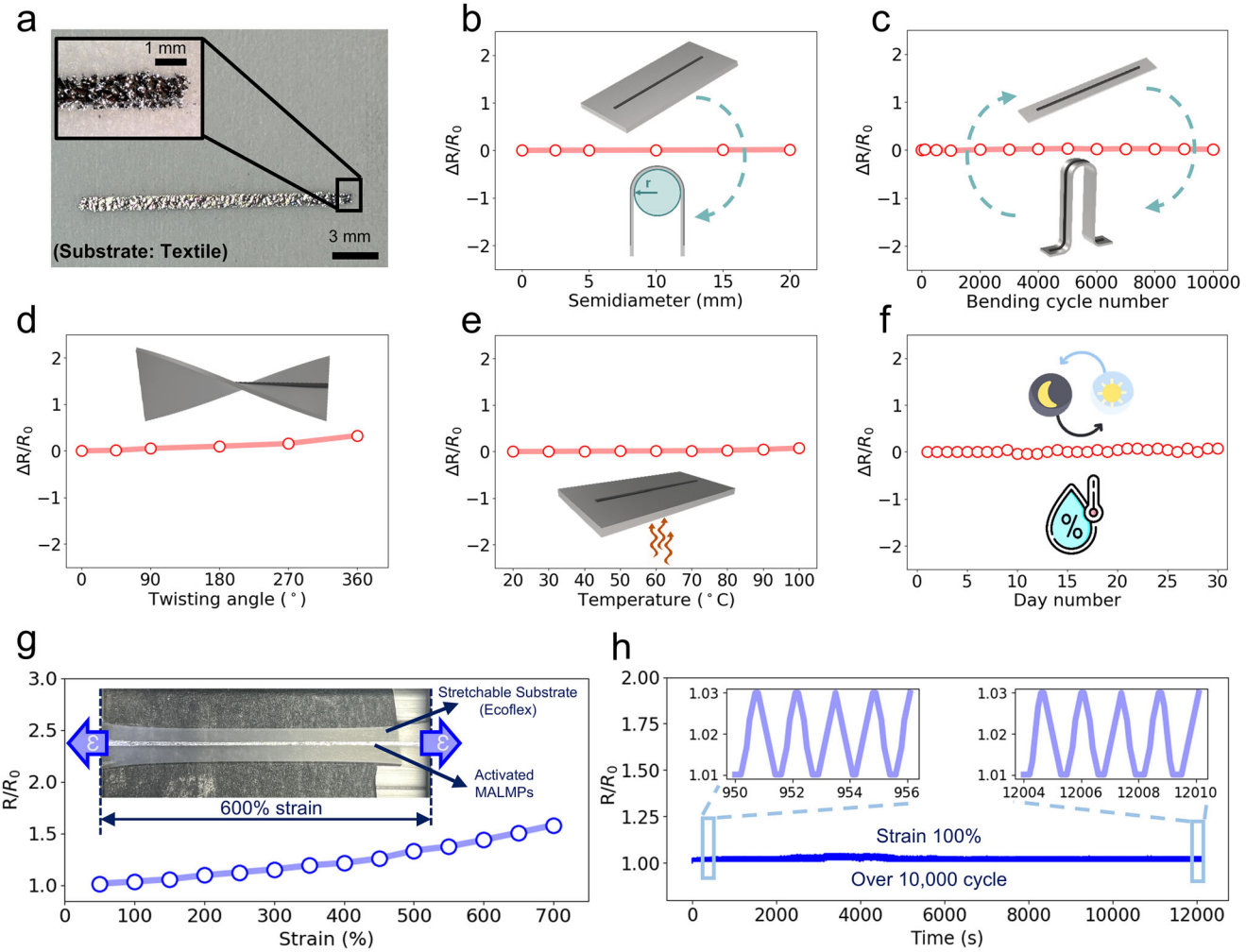


Figure 5. Mechanical, electrical, and environmental durability, substrate adaptability, and recyclability of MALMPs-based conductive electrodes. a) Image of an MALMPs electrode on a non-woven textile. b) Relative resistance change ($\Delta R/R_0$) as a function of bending radius, demonstrating negligible resistance variation down to a bending radius of 2.5 mm. c) Electrical durability under 10 000 bending cycles with a curvature radius of 10 mm, showing excellent mechanical fatigue resistance. d) Resistance stability under repeated twisting cycles over 360°, confirming torsional robustness. e) Electrical response under increasing temperatures (25–100 °C), demonstrating thermal stability. f) Ambient aging behavior over 30 days under ambient humidity, confirming long-term environmental durability. g) Stretchability test of MALMPs electrodes on Ecoflex, exhibiting moderate resistance increase while maintaining electrical functionality up to 700% strain. h) Electromechanical cycling performance under 100% strain for over 10 000 cycles. Insets showing expanded resistance response at the beginning and end of the test, indicating stable performance.

≈1.55 (Figure 5g). Under continuous cyclic strain of 100% over 10 000 loading cycles, the MALMPs electrode exhibited stable electrical performance, with normalized resistance remaining within the range of 1.00 to 1.03, corresponding to a modest variation of 3%, indicating excellent electrical consistency. (Figure 5h). Insets show expanded resistance profiles at both the beginning and end of the test, confirming high electromechanical resilience and excellent fatigue resistance.

2.5. MALMPs-Based Transient, Reconfigurable, and Wearable Electronics

MALMPs enable a broad range of electronic functionalities, as demonstrated through a series of transient, reconfigurable, and skin-integrated systems that underscore their recyclability, versatility, and suitability for on-skin applications. To demonstrate the full recyclability of the MALMPs system as a platform for transient electronics, we established a closed-loop regeneration process (**Figure 6a**; Figures S15 and S16, Supporting Information). Transient circuits were first fabricated using printed MALMPs and subsequently dissolved in water. The dissolved residues were then treated with NaOH to recover EGaIn in its liquid phase, which can be re-synthesized into MALMPs via sonication. This regenerative cycle was validated in real time by dissolving a printed circuit, collecting the recovered EGaIn (Movie S7, Supporting Information). Building on pressure-triggered activation capability, we developed an on-demand reconfigurable pulse-sensing module, further highlighting the versatility of MALMPs in wearable bioelectronics. The system comprises a

© 2025 Wiley-VCH GmbH

16163028, 2026, 22, Downloaded from https://advanced.onlinelibrary.wiley.com/doi/10.1002/adfm.202527396 by Korea University Library, Wiley Online Library on [29/03/2026]. See the Terms and Conditions (https://onlinelibrary.wiley.com/terms-and-conditions) on Wiley Online Library for rules of use; OA articles are governed by the applicable Creative Commons License

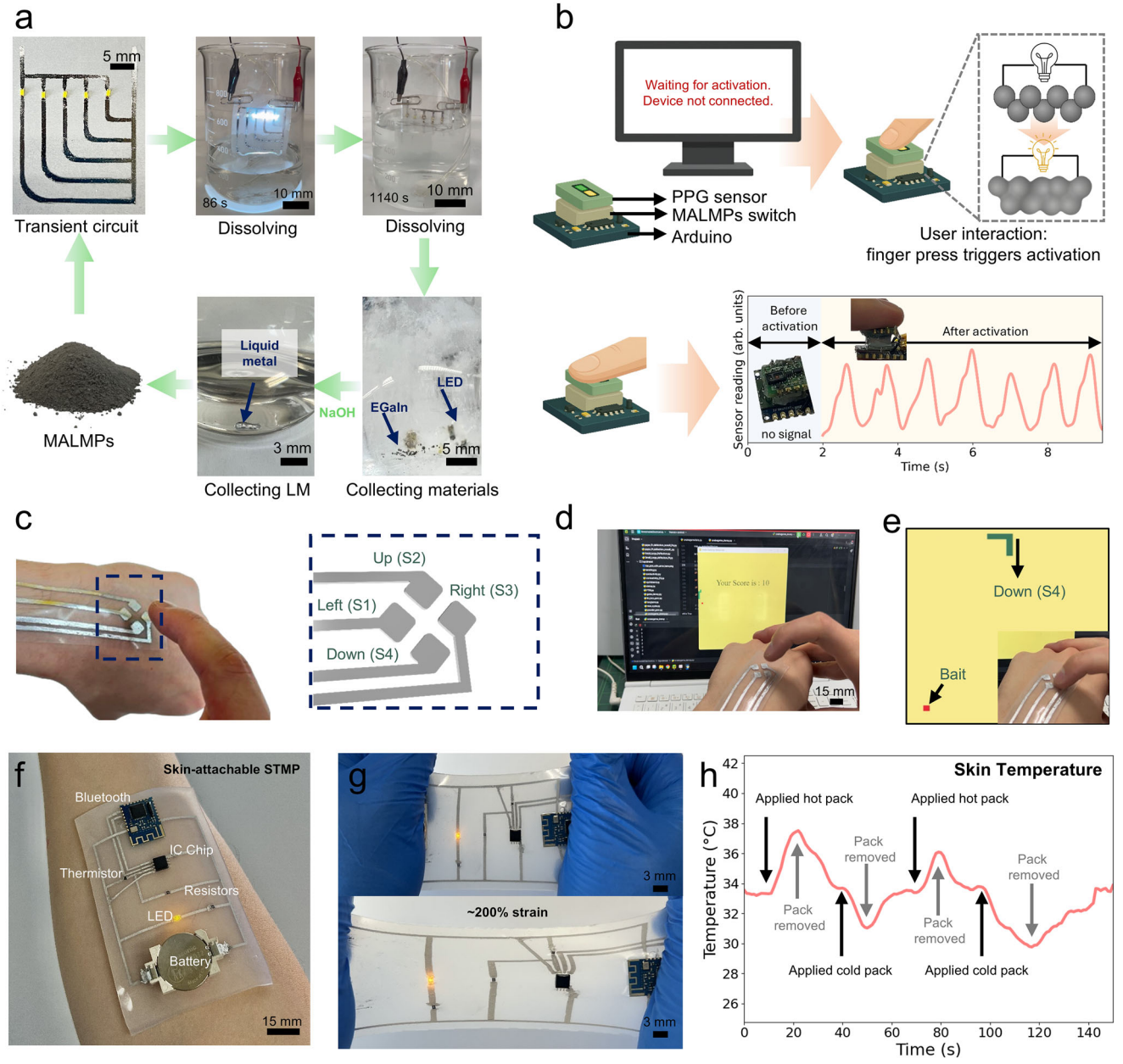


Figure 6. Multifunctional capabilities of MALMPs-based electronics for transient, reconfigurable, and wearable applications. a) Real-time photographic sequence showing the dissolution of an MALMPs-based circuit in water and subsequent EGaIn recovery with NaOH, and transformation back into MALMPs, validating the full recyclability of the system. b) Schematic illustration of the on-demand reconfigurable pulse sensing module composed of a photoplethysmographic (PPG) sensor, MALMPs switch layer, and Arduino. In the initial state, the MALMPs layer remains electrically insulating, effectively blocking current flow and disabling device operation. Upon mechanical activation, the MALMPs transition to a conductive state, reconfiguring the circuit and enabling full device functionality. The user initiates device activation by applying localized finger pressure, triggering the MALMPs-based switch to transition from an electrically insulating to a conductive state. This reconfiguration enables circuit completion on demand, powering the device and initiating wireless data transmission via Bluetooth. The activated system subsequently acquires and transmits real-time pulse signals for monitoring. c) Photograph and schematic illustration of a skin-conformal capacitive sensor array interfaced with a human finger. d,e) Functional demonstration of the skin-mounted sensor, where finger touches activate direction control in a capacitive-input-based game interface. The device is used to play a snake game through capacitive input. f) Real image of the stretchable temperature monitoring patch (STMP) device conformally attached to skin. g) Photograph of the STMP device under ≈200% mechanical strain. f) Real-time wireless temperature readings transmitted from the STMP under different thermal stimuli (cold pack and warm surface).

© 2025 Wiley-VCH GmbH

16163028, 2026, 22, Downloaded from https://advanced.onlinelibrary.wiley.com/doi/10.1002/adfm.202527396 by Korea University Library, Wiley Online Library on [29/03/2026]. See the Terms and Conditions (https://onlinelibrary.wiley.com/terms-and-conditions) on Wiley Online Library for rules of use; OA articles are governed by the applicable Creative Commons License

photoplethysmographic (PPG) sensor, a MALMPs switch layer, and a microcontroller (Arduino) (Figure 6b). In the initial, inactivated state, the MALMPs remain electrically insulating, effectively preventing current flow and keeping the device powered off. Upon applying localized mechanical pressure, such as a finger press, the oxide shells of the MALMPs in the switch layer rupture, causing the material to become conductive and complete the circuit (Movie S8, Supporting Information). This reconfiguration restores power to the sensing module and initiates wireless data transmission via Bluetooth. The device successfully acquires and transmits real-time pulse waveforms (Movie S9, Supporting Information), demonstrating a user-triggered, secure, and reconfigurable sensing platform based on MALMPs.

We further demonstrated skin-conformal electronic interactions enabled by MALMPs through the development of a wearable capacitive sensor array for human–machine interfacing. Four MALMPs-based directional electrodes (S1–S4) were brush-patterned onto an Ecoflex substrate using a laser-cut PET mask and conformally attached to the skin (Figure 6c). When integrated with a capacitive touch module, this soft interface enabled directional input through finger pressing. As a representative demonstration, the system was used to control a classic snake game in real time, with each electrode mapped to a movement direction (Figure 6d,e; Movie S10, Supporting Information), highlighting the programmability and responsiveness of the MALMPs-based circuit. Expanding the multifunctional scope of MALMP-based circuitry, we developed a skin-conformal, wireless, and stretchable temperature monitoring patch (STMP) (Figure S17 and Movie S11, Supporting Information). The circuit layout was patterned in three conductive layers using sequential brush printing guided by laser-cut masks and encapsulated in soft Ecoflex (Figure 6f; Figure S18, Supporting Information). The STMP integrates MALMPs-based interconnects with surface-mounted electronics, including a thermistor, IC chip, Bluetooth module, and LED indicator (Figure S19, Supporting Information), forming a fully soft and wireless temperature sensing system. The device was also robust under significant mechanical deformation, maintaining full functionality up to ≈200% strain without delamination or electrical failure (Figure 6g; Movie S12, Supporting Information). The skin-mounted STMP exhibited stable wireless transmission of real-time temperature data under repeated thermal perturbations, such as hot/cold pack application (Figure 6h), confirming its utility for physiological monitoring. These results underscore the potential of MALMPs for scalable, reconfigurable, and body-integrated bioelectronic systems.

3. Conclusion

We introduced a sustainable and scalable fabrication strategy for versatile electronics through MALMPs. Unlike conventional LMs that suffer from high surface tension and require encapsulation or post-treatment for functional retention, our MALMPs system leverages solvent-mediated oxide stabilization and pressure-triggered conductivity to achieve ambient-stable, recyclable, and reconfigurable versatile circuitry. The dry-state MALMPs remain electrically inert until mechanically activated, enabling on-demand patterning across diverse platforms such as rigid wafers, flexible substrates, polymers, porous, and bio-derived substrates. This substrate versatility, combined with simple patterning methods such as stamping and brushing, supports rapid integration into conformal and 3D electronics. Importantly, the system supports full recyclability: printed circuits can be chemically dissolved, with pristine LMs recovered and regenerated without compromising performance. This closed-loop process reduces material waste and aligns with growing demands for environmentally responsible electronic manufacturing. Beyond the material and process-level innovations, the functional demonstration, from skin-conformal sensors to pressure-triggered reconfigurable interfaces, highlights the broad applicability of MALMPs in wearable healthcare, transient electronics, and adaptive IoT systems. By integrating pressure-activated switching into soft devices, this platform enables a new class of user-interactive electronics in which circuit functionality can be defined, reconfigured, or erased on demand. Future work will focus on engineering the oxide shell composition and microstructure to finely tune the mechanical activation threshold, enabling application-specific responses, from ultra-soft touch interfaces to mechanically gated logic. Expanding the chemical scope of coordinating solvents may also allow surface functionalization for targeted adhesion or stimuli-responsiveness. Integration with functional soft materials, such as hydrogels, biodegradable polymers, or responsive elastomers, could extend the platform to implantable, bioresorbable, or environmentally adaptive electronics. These advances position MALMPs as a foundational material platform for next-generation electronics, offering a unique combination of reconfigurability, recyclability, and compatibility with emerging biointegrated and sustainable technologies.

4. Experimental Section

These experiments were approved by the institutional review board (IRB) of the Korea Advanced Institute of Science and Technology (KAIST) (IRB no. KH2024-200).

Materials: LM alloy (eutectic gallium–indium, EGaIn) was purchased from Santech Material. The solvents were obtained from Daejung Chemical & Metals. Substrates of A4 paper, PET (polyethylene glycol terephthalate), PMMA (Poly(methyl methacrylate)), PI (polyimide), PVC(Polyvinyl chloride), PE (Polyethylene), and PP (Polypropylene), and Glass were purchased from Coupang. The textile was WW-2109 purchased by KM Corp. These textiles are described by the manufacturer as being made of Polyester (45%) and Cellulose (%55).

Fabrication and Recycling Process of MALMPs: To synthesize MALMPs, eutectic gallium–indium (EGaIn; Santech Materials, China) and an organic solvent (Daejung Chemical & Metals, Korea) were mixed in a 1:1 volume ratio and sealed in a glass vial. The mixture was sonicated in a bath sonicator for 3 h at ambient temperature to promote solvent-assisted dispersion. After sonication, the solution was transferred to a vacuum convection oven and dried overnight to enable complete solvent evaporation. The resulting powder was gently agitated to disperse aggregated clusters, yielding dry, free-flowing MALMPs. Notably, the fabricated MALMPs can be chemically recycled by dissolving them in a mildly diluted sodium hydroxide solution, prepared by mixing 30 wt% NaOH stock solution (Daejung Chemical & Metals) with deionized water at a 1:10 ratio. The recycling process was performed at room temperature, and the oxide shell dissolves immediately upon introduction of the MALMPs into the recycling bath, as shown in Movie S13, Supporting Information, rapidly releasing the pristine liquid metal core. Importantly, this immediate conversion back to liquid EGaIn occurs for both freshly prepared samples (1 day old) and powders stored for up to 1 year, demonstrating consistent recyclability regardless of storage duration.

© 2025 Wiley-VCH GmbH

16163028, 2026, 22, Downloaded from https://advanced.onlinelibrary.wiley.com/doi/10.1002/adfm.202527396 by Korea University Library, Wiley Online Library on [29/03/2026]. See the Terms and Conditions (https://onlinelibrary.wiley.com/terms-and-conditions) on Wiley Online Library for rules of use; OA articles are governed by the applicable Creative Commons License

Fabrication of Recyclable Circuits: Brush-patterning masks were fabricated via UV laser cutting. The desired patterns were designed using a 3D computer-aided design (CAD) program (Fusion 360, Autodesk, USA) and exported as DXF files. These files were then imported into the UV laser marking software (Marking Builder, KEYENCE, Japan) for mask fabrication. PET films were used as the mask substrate and patterned using a UV laser system (MD-U1000C, KEYENCE, Japan). After cutting, the patterned PET masks were peeled from the film and aligned onto the target substrate. To establish the transient circuitry, a water-soluble paper (Aquasol, USA) was used as the target substrate. MALMPs were then manually brushed across the mask to deposit patterned traces onto the underlying substrate. Following pattern formation, electronic components such as LEDs were placed and affixed using a silicone adhesive (Sil-Poxy; Figure S16, Supporting Information).

Fabrication Process of Human–Machine Interface Device: To fabricate the human–machine interface (HMI) device, a laser-patterned PET mask was first placed onto an Ecoflex (Smooth-On, USA) substrate (thickness: 100 µm). LMP particles were then applied via brushing through the patterned mask to form conductive traces on the Ecoflex surface. After completing the circuit patterning, the flexible device was gently removed and directly attached to the skin for operation. A capacitive touch sensing module (MPR121, Adafruit) was integrated to detect input signals, enabling real-time directional control of a digital snake game through skin-based touch gestures.

Fabrication Process of STMP: Ecoflex-0030 (Smooth-On Inc., USA) was first spin-coated onto a 150 × 150 mm soda-lime glass substrate to form the base elastomeric layer. A laser-patterned PET mask (1st mask) was then aligned and attached to the cured surface, followed by brush-based deposition of MALMPs to form the first conductive layer (Figure S19a, Supporting Information). A second layer of Ecoflex-0030 was subsequently spin-coated to encapsulate the initial circuit. After curing, a second PET mask (2nd mask) was applied, and additional MALMPs were brushed onto the new surface to define the second conductive layer. Electronic components, excluding the battery, were then placed and embedded into the structure. A third Ecoflex-0030 layer was spin-coated to serve as the final encapsulation layer. Finally, a third PET mask (3rd mask) was aligned, and MALMPs were applied via brushing to complete the topmost conductive traces. The battery was affixed using Sil-Poxy adhesive (Smooth-On, USA), and the entire multilayer device was gently peeled off from the soda-lime glass substrate for use (Figure S19b, Supporting Information).

Fabrication Process of an On-Demand Reconfigurable Device: A 3D-printed mold was fabricated using fused deposition modeling (FDM) with poly(lactic acid) (PLA) filament to cast Ecoflex (Smooth-On, USA) and form a recessed cavity designed to house the MALMPs switch (Figure S20, Supporting Information). After curing, the Ecoflex mold was demolded, and the mechanochemically activatable MALMPs were deposited into the cavity. The structure was then sealed using Sil-Poxy (Smooth-On, USA) to ensure mechanical stability and safe encapsulation of the conductive powder. The complete system integrates a MAX30101 photoplethysmographic (PPG) sensor (Maxim Integrated Products, Inc), an Arduino Nano 33 BLE microcontroller, a 3.7 V Li–Po battery, and the fabricated MALMPs switch, all electrically connected to create a compact sensing module. Upon finger-pressure-induced activation of the MALMP switch, the circuit is completed, enabling device operation. Real-time biosignal data were wirelessly transmitted via Bluetooth Low Energy (BLE) and received on a host computer using a custom Python GUI (PyCharm IDE, JetBrains), where pulse signals were visualized and monitored.

Characterization—Morphological Characterization: The surface morphology and internal structure of the MALMPs were examined using transmission electron microscopy (TEM; Tecnai F20, FEI, USA). Prior to imaging, the MALMPs were diluted in ethanol and drop-cast onto 400-mesh copper grids. To minimize oxidation artifacts and ensure accurate measurement of the native oxide shell, all samples were prepared and imaged within 1 h of deposition. This protocol allowed for reliable evaluation of the core–shell structure and oxide layer thickness of the MALMPs.

Characterization—Chemical Characterization: Fourier-transform infrared spectroscopy (FTIR) analysis was performed using a Nicolet iS50 FTIR spectrometer (Thermo Fisher Scientific, USA) to investigate the chemical functionalities present on the surface of the MALMPs. X-ray photoelectron spectroscopy (XPS) measurements were conducted using a Nexsa G2 system (Thermo Scientific, USA) under in situ conditions. High-resolution spectra were collected to evaluate the chemical bonding states and confirm solvent coordination and oxide formation on the particle surfaces. X-ray diffraction (XRD) patterns of the LMPs were obtained using a SmartLab diffractometer (RIGAKU, Japan) to examine the crystalline phases and long-term structural stability of the powders.

Characterization—Electrical Characterization: The electrical properties of the MALMPs-based conductors were measured using a four-point probe configuration connected to a source meter unit (2400, Keithley, USA). To evaluate resistance changes under mechanical strain, a universal testing machine (AG-X Plus, Shimadzu, Japan) equipped with a 1 kN load cell (SBL-1KN, Shimadzu, Japan) was employed. Pneumatic flat grips (Shimadzu, Japan) were used to ensure consistent and secure clamping of the specimens during testing.

Supporting Information

Supporting Information is available from the Wiley Online Library or from the author.

Acknowledgements

I.P. was supported by the National Research Foundation of Korea (NRF) grant funded by the Korean government (MSIT) (No. 2021R1A2C3008742).

H.J.K. was supported by the Korea Evaluation Institute of Industrial Technology (KEIT) grant funded by the Korea government (MOTIE, Grant No. RS-2022-00154781, Development of large-area wafer-level flexible/stretchable hybrid sensor platform technology for form-factor-free highly integrated convergence sensor).

Conflict of Interest

The authors declare no conflict of interest.

Data Availability Statement

The data that support the findings of this study are available in the supplementary material of this article.

Keywords

liquid metals, reconfigurable electronics, recyclable electronics, stretchable electronics, universal substrate

Received: October 14, 2025
Revised: November 18, 2025
Published online: December 10, 2025

[1] O. Gul, M. Song, C.-Y. Gu, J. Ahn, K. Lee, J. Ahn, H. J. Kim, T.-S. Kim, I. Park, *Nat. Commun.* **2025**, *16*, 1337.
[2] H. Seo, G.-H. Lee, J. Park, D.-Y. Kim, Y. Son, S. Kim, K. S. Nam, C. Yang, J. Won, J.-Y. Bae, H. Kim, S.-K. Kang, S. Park, J. Kang, S. Park, *Nat. Commun.* **2025**, *16*, 4944.
[3] O. Gul, M. Song, C.-Y. Gu, J. Ahn, K. Lee, T.-S. Kim, J. Ahn, H. J. Kim, I. Park, *Small* **2025**, *21*, 2410247.

© 2025 Wiley-VCH GmbH

16163028, 2026, 22, Downloaded from https://advanced.onlinelibrary.wiley.com/doi/10.1002/adfm.202527396 by Korea University Library, Wiley Online Library on [29/03/2026]. See the Terms and Conditions (https://onlinelibrary.wiley.com/terms-and-conditions) on Wiley Online Library for rules of use; OA articles are governed by the applicable Creative Commons License

[4] J. Jang, H. Choo, S. Lee, J. Song, K. Park, J. Yoon, D. Seong, S. An, H. Jung, J. Ju, J. Kang, J. Kang, I. S. Kim, M. Shin, J.-H. Park, D. Son, *Nat. Electron.* **2025**, *8*, 474.
[5] T. Wang, J. Meng, X. Zhou, Y. Liu, Z. He, Q. Han, Q. Li, J. Yu, Z. Li, Y. Liu, H. Zhu, Q. Sun, D. W. Zhang, P. Chen, H. Peng, L. Chen, *Nat. Commun.* **2022**, *13*, 7432.
[6] K. Kim, J. Kim, M. Jung, I. S. Kim, B.-S. Yu, S. M. Won, D. Son, H. Li, Z. Sofer, D. K. Hwang, D. Jariwala, J. Kang, *Nat. Electron.* **2025**, *8*, 461.
[7] N. X. Williams, G. Bullard, N. Brooke, M. J. Therien, A. D. Franklin, *Nat. Electron.* **2021**, *4*, 261.
[8] C. H. Dreimol, H. Guo, M. Ritter, T. Keplinger, Y. Ding, R. Günther, E. Poloni, I. Burgert, G. Panzarasa, *Nat. Commun.* **2022**, *13*, 3680.
[9] Z. Zhang, A. K. Biswal, A. Nandi, K. Frost, J. A. Smith, B. H. Nguyen, S. Patel, A. Vashisth, V. Iyer, *Nat. Sustain.* **2024**, *7*, 616.
[10] J. Ahn, J.-S. Kim, Y. Jeong, S. Hwang, H. Yoo, Y. Jeong, J. Gu, M. Mahato, J. Ko, S. Jeon, J.-H. Ha, H.-S. Seo, J. Choi, M. Kang, C. Han, Y. Cho, C. H. Lee, J.-H. Jeong, I.-K. Oh, I. Park, *Adv. Energy Mater.* **2022**, *12*, 2201341.
[11] X. Gao, X. Chen, M. Lin, W. Yue, H. Hu, S. Qin, F. Zhang, Z. Lou, L. Yin, H. Huang, S. Zhou, Y. Bian, X. Yang, Y. Zhu, J. Mu, X. Wang, G. Park, C. Lu, R. Wang, R. S. Wu, J. Wang, J. Li, S. Xu, *Nat. Electron.* **2024**, *7*, 1035.
[12] Y. Lee, J. W. Chung, G. H. Lee, H. Kang, J.-Y. Kim, C. Bae, H. Yoo, S. Jeong, H. Cho, S.-G. Kang, J. Y. Jung, D.-W. Lee, S. Gam, S. G. Hahm, Y. Kuzumoto, S. J. Kim, Z. Bao, Y. Hong, Y. Yun, S. Kim, *Sci. Adv.* **2021**, *7*, abg9180.
[13] B. Lee, H. Cho, S. Moon, Y. Ko, Y.-S. Ryu, H. Kim, J. Jeong, S. Chung, *Nat. Electron.* **2023**, *6*, 307.
[14] K. Lee, O. Gul, Y. Kwon, J. Jeong, S. Cho, J. Ahn, J. Yu, C. Kim, D. Lee, H. Han, B. Lee, J. Choi, J.-H. Ha, Y. Jeong, K. Kang, A. Javey, J. Ahn, I. Park, *Adv. Funct. Mater.* **2025**, https://doi.org/10.1002/adfm.202519859.
[15] M. Cianchetti, C. Laschi, A. Menciassi, P. Dario, *Nat. Rev. Mater.* **2018**, *3*, 143.
[16] D. Hu, F. Giorgio-Serchi, S. Zhang, Y. Yang, *Nat. Mach. Intell.* **2023**, *5*, 261.
[17] V. Cacucciolo, J. Shintake, Y. Kuwajima, S. Maeda, D. Floreano, H. Shea, *Nature* **2019**, *572*, 516.
[18] Y. Hong, K. Jia, Y. Zhang, Z. Li, J. Jia, J. Chen, Q. Liang, H. Sun, Q. Gao, D. Zhou, R. Li, X. Dong, X. Fan, S. He, *Nat. Commun.* **2024**, *15*, 9539.
[19] F. Jin, T. Li, Z. Wei, L. Qian, N. Javanmardi, T. Wang, S. Wang, Z.-Q. Feng, *Nat. Rev. Electr. Eng.* **2025**, *2*, 338.
[20] C. Yang, P. Li, C. Wei, A. Prominski, J. Ma, C. Sun, J. Yue, Z. Cheng, J. Zhang, B. Ashwood, W. Li, J. Shi, K. Hou, F. Shi, P. Griffin, L. Jin, B. Tian, *Nat. Sustain.* **2024**, *7*, 1190.
[21] S. Lee, S. A. Jaseem, N. Atar, M. Wang, J. Y. Kim, M. Zare, S. Kim, M. D. Bartlett, J.-W. Jeong, M. D. Dickey, *Chem. Rev.* **2025**, *125*, 3551.
[22] Y. Lin, J. Genzer, M. D. Dickey, *Adv. Sci.* **2020**, *7*, 2000192.
[23] T. V. Neumann, M. D. Dickey, *Adv. Mater. Technol.* **2020**, *5*, 2000070.
[24] S. Chen, H.-Z. Wang, R.-Q. Zhao, W. Rao, J. Liu, *Matter* **2020**, *2*, 1446.
[25] M. D. Dickey, *Adv. Mater.* **2017**, *29*, 1606425.
[26] O. Gul, J. Kim, K. Kim, H. J. Kim, I. Park, *Adv. Mater. Technol.* **2024**, *9*, 2302134.
[27] K. Kim, J. Ahn, Y. Jeong, J. Choi, O. Gul, I. Park, *Micro Nano Syst. Lett.* **2021**, *9*, 2.
[28] O. Gul, K. Kim, J. Gu, J. Choi, D. Del Orbe Henriquez, J. Ahn, I. Park, *ACS Appl. Electron. Mater.* **2021**, *3*, 4027.
[29] H. Park, K. Kim, S.-J. Kweon, O. Gul, J. Choi, Y. S. Oh, I. Park, M. Je, *IEEE Trans. Biomed. Circuits Syst.* **2023**, *17*, 889.
[30] Q. Zhuang, K. Yao, M. Wu, Z. Lei, F. Chen, J. Li, Q. Mei, Y. Zhou, Q. Huang, X. Zhao, Y. Li, X. Yu, Z. Zheng, *Sci. Adv.* **2023**, *9*, adg8602.
[31] Q. Zhuang, K. Yao, C. Zhang, X. Song, J. Zhou, Y. Zhang, Q. Huang, Y. Zhou, X. Yu, Z. Zheng, *Nat. Electron.* **2024**, *7*, 598.
[32] S. Liu, M. C. Yuen, E. L. White, J. W. Boley, B. Deng, G. J. Cheng, R. Kramer-Bottiglio, *ACS Appl. Mater. Interfaces* **2018**, *10*, 28232.
[33] S. Liu, S. Y. Kim, K. E. Henry, D. S. Shah, R. Kramer-Bottiglio, *ACS Appl. Mater. Interfaces* **2021**, *13*, 28729.
[34] S. Liu, S. N. Reed, M. J. Higgins, M. S. Titus, R. Kramer-Bottiglio, *Nanoscale* **2019**, *11*, 17615.
[35] E. J. Markvicka, M. D. Bartlett, X. Huang, C. Majidi, *Nat. Mater.* **2018**, *17*, 618.
[36] C. J. Thrasher, Z. J. Farrell, N. J. Morris, C. L. Willey, C. E. Tabor, *Adv. Mater.* **2019**, *31*, 1903864.
[37] X. Li, M. Li, L. Zong, X. Wu, J. You, P. Du, C. Li, *Adv. Funct. Mater.* **2018**, *28*, 1804197.
[38] K. Zheng, F. Gu, H. Wei, L. Zhang, X. Chen, H. Jin, S. Pan, Y. Chen, S. Wang, *Small Methods* **2023**, *7*, 2201534.
[39] M.d.A. Rahim, F. Centurion, J. Han, R. Abbasi, M. Mayyas, J. Sun, M. J. Christoe, D. Esrafilzadeh, F.-M. Allioux, M. B. Ghasemian, J. Yang, J. Tang, T. Daeneke, S. Mettu, J. Zhang, M. H. Uddin, R. Jalili, K. Kalantar-Zadeh, *Adv. Funct. Mater.* **2021**, *31*, 2007336.
[40] Y. Zheng, H. Liu, L. Yan, H. Yang, L. Dai, C. Si, *Adv. Funct. Mater.* **2024**, *34*, 2310653.
[41] S. Veerapandian, W. Jang, J. B. Seol, H. Wang, M. Kong, K. Thiyagarajan, J. Kwak, G. Park, G. Lee, W. Suh, I. You, M. E. Kılıç, A. Giri, L. Beccai, A. Soon, U. Jeong, *Nat. Mater.* **2021**, *20*, 533.
[42] D. H. Ho, C. Hu, L. Li, M. D. Bartlett, *Nat. Electron.* **2024**, *7*, 1015.
[43] D. H. Ho, M. Jiang, R. Tutika, J. C. Worch, M. D. Bartlett, *Adv. Mater.* **2025**, *37*, 2501341.
[44] A. Martin, C. Du, B. Chang, M. Thuo, *Chem. Mater.* **2020**, *32*, 9045.
[45] K. Zuraiqi, A. Zavabeti, F.-M. Allioux, J. Tang, C. K. Nguyen, P. Tafazolymotie, M. Mayyas, A. V. Ramarao, M. Spencer, K. Shah, C. F. McConville, K. Kalantar-Zadeh, K. Chiang, T. Daeneke, *Joule* **2020**, *4*, 2290.
[46] A. Goff, P. Aukarasereenont, C. K. Nguyen, R. Grant, N. Syed, A. Zavabeti, A. Elbourne, T. Daeneke, *Dalton Trans.* **2021**, *50*, 7513.
[47] H. Bark, P. S. Lee, *Chem. Sci.* **2021**, *12*, 2760.
[48] P. H. A. Vaillant, V. Krishnamurthi, C. J. Parker, R. Kariuki, S. P. Russo, A. J. Christofferson, T. Daeneke, A. Elbourne, *Adv. Funct. Mater.* **2024**, *34*, 2310147.
[49] J. Pyeon, H. Lee, W. Choe, S. Park, H. Kim, *Small* **2025**, *21*, 2501829.

© 2025 Wiley-VCH GmbH

16163028, 2026, 22, Downloaded from https://advanced.onlinelibrary.wiley.com/doi/10.1002/adfm.202527396 by Korea University Library, Wiley Online Library on [29/03/2026]. See the Terms and Conditions (https://onlinelibrary.wiley.com/terms-and-conditions) on Wiley Online Library for rules of use; OA articles are governed by the applicable Creative Commons License